

# Disparities between in situ and optically-derived carbon biomass and growth rates of the prymnesiophyte *Phaeocystis globosa*

3

4 L. Peperzak<sup>1,2</sup>, H. J. van der Woerd<sup>1</sup> and K. R. Timmermans<sup>2</sup>

5 [1] [Institute for Environmental Studies (IVM), VU University Amsterdam, The Netherlands]

[2] [Royal Netherlands Institute for Sea Research / NIOZ, Department of Biological  
Oceanography, Texel, The Netherlands]

8

9 Correspondence to: L. Peperzak ([Louis.Peperzak@nioz.nl](mailto:Louis.Peperzak@nioz.nl))

10

## 11 Abstract

12 The oceans play a pivotal role in the global carbon cycle. It is not practical to measure the  
13 global daily production of organic carbon, the product of phytoplankton standing stock and  
14 growth rate by discrete oceanographic methods. Instead, optical proxies from Earth-orbiting  
15 satellites must be used. To test the accuracy of optically-derived proxies of phytoplankton  
16 physiology and growth rate, hyperspectral reflectance data from the wax and wane of a  
17 *Phaeocystis* bloom in laboratory mesocosms were compared with standard ex situ data.  
18 Chlorophyll biomass could be estimated accurately from reflectance using specific  
19 chlorophyll absorption algorithms. However, the conversion of chlorophyll (Chl) to carbon  
20 (C) was obscured by the non-linear increase in C:Chl under nutrient-limited growth. Although  
21 C:Chl was inversely correlated ( $r^2=0.88$ ) with the in situ fluorometric growth rate indicator  
22 Fv/Fm (Photosystem II quantum efficiency), none of them was linearly correlated to growth

- 1 rate, constraining the accurate calculation of *Phaeocystis* growth or production rates.
- 2 Unfortunately, the optical proxy  $\varphi_{ph}$  (quantum efficiency of fluorescence: the ratio of the
- 3 number of fluoresced photons to the number of photons absorbed by the phytoplankton) did
- 4 not show any correlation with *Phaeocystis* growth rate and, therefore, it is concluded that  $\varphi_{ph}$
- 5 cannot be applied in the remote-sensed measurement of this species' carbon production rate.

## 1 Introduction

1

2     Approximately half of the global photosynthetic CO<sub>2</sub> to organic carbon conversion takes  
3     place in marine waters (Field et al., 1998). Unfortunately, global daily CO<sub>2</sub> fixation, the  
4     product of phytoplankton standing stock and growth rates cannot be measured directly for the  
5     world oceans. Phytoplankton biomass and growth rates can be assessed directly and  
6     accurately by standard oceanographic techniques, but these miss the spatial coverage of the  
7     optical instruments on board Earth-orbiting satellites. On the other hand, optically-derived  
8     estimates of phytoplankton biomass and growth rates are less accurate than ship-board data  
9     (Abbott and Letelier, 1999;Carder et al., 2003;Behrenfeld et al., 2005;Huot et al.,  
10    2005;Astoreca et al., 2009;Martinez-Vicente et al., 2013). Here we report, to our knowledge  
11    for the first time ever, on the simultaneous evaluation of standard oceanographic and state-of-  
12    the-art optical techniques for gauging both phytoplankton biomass and carbon growth rates.

13    In “standard” oceanographic measurements, carbon concentration, carbon fixation,  
14    chlorophyll and other photopigment concentrations are analysed in discrete water samples (ex  
15    situ), as is the quantum efficiency of Photosystem II (Fv/Fm) that can be considered an  
16    indicator for phytoplankton growth rate (Kromkamp and Foster, 2003;Ly et al., 2014).

17    Optical estimates of the oceanic carbon concentration for growth rate estimations can be made  
18    from the particulate backscatter coefficient bbp (Behrenfeld et al., 2005), but this coefficient  
19    is non-specific for phytoplankton or valid only for low chlorophyll-a concentrations  
20    (Martinez-Vicente et al., 2013). Alternatively, the phytoplankton-specific chlorophyll  
21    concentration can be estimated from water-leaving radiance as absorbance (Carder et al.,  
22    2003). However, the carbon to chlorophyll ratio (C : Chl) that is then needed to convert  
23    chlorophyll into carbon is not a constant (Sathyendranath et al., 2009).

1 A second optical growth rate proxy is the phytoplankton-specific red chlorophyll fluorescence  
2 relative to absorbance ( $\phi_{ph}$ ). By definition this “quantum efficiency of fluorescence” is the  
3 ratio of the number of fluoresced photons to the number of photons absorbed by the  
4 phytoplankton, i.e. by all cellular photo-pigments (Abbott and Letelier, 1999;Huot et al.,  
5 2005). According to Falkowski and Kolber (Falkowski and Kolber, 1995) the quantum  
6 efficiency of photosynthesis varies inversely to the quantum efficiency of fluorescence. If  
7 under nutrient limitation the production of chlorophyll stops, it is expected that C: Chl,  
8 fluorescence and  $\phi_{ph}$  will increase (Kiefer, 1973;Falkowski et al., 1992;Behrenfeld et al.,  
9 2009).

10 Besides the lack of specificity, an inherent problem in the optical approach of organic carbon  
11 production is that estimates of carbon and chlorophyll are used in both biomass and growth  
12 rate proxies. Moreover, doubt has been raised if the variability in remote-sensed  
13 phytoplankton physiology ( $\phi_{ph}$ ) is due to physiological changes in the phytoplankton, or due  
14 to environmentally driven biases in algorithms needed to estimate  $\phi_{ph}$  (Huot et al., 2005).

15 In order to study the variability in phytoplankton biomass, growth rate, absorbance and  
16 fluorescence under variable, but fully-controlled conditions, a mesocosm experiment was  
17 conducted where detailed “standard” oceanographic measurements were combined with  
18 close-sensing hyperspectral measurements. Phytoplankton dynamics in the mesocosms were  
19 experimentally manipulated under semi-natural conditions of temperature, irradiance and  
20 turbulence (Peperzak et al., 2011). The prymnesiophyte *Phaeocystis globosa*, a key species in  
21 marine primary production was used as test organism (Wassmann et al., 1990;Smith et al.,  
22 1991;DiTullio et al., 2000;Vogt et al., 2012). Our ambition was to use the optical signature of  
23 *Phaeocystis globosa*, that can now be detected by the MERIS and MODIS satellites (Kurekin,  
24 2014), to better understand the wax and wane of its blooms. This optical signature includes  
25 light absorption, light emission and the quantum efficiency of the phytoplankton. In

1 particular we like to know how optical proxies compare to standard oceanographic techniques  
2 for estimating primary production because this is still one of the key question in ocean color  
3 research (Cullen and Lewis, 1995;Saba and al., 2010;Huot et al., 2013;Behrenfeld et al.,  
4 2009;Huot et al., 2005).

5

## 6 **2 Methods**

### 7 **2.1 Experimental**

8 The flagellate, not-colony-forming, strain Pg6-I of *Phaeocystis globosa* (“*Phaeocystis*”) was  
9 inoculated in two duplicate 140 L mesocosms filled with 0.2  $\mu\text{m}$  filtered Atlantic Ocean water  
10 poor in organic and inorganic nutrients that had been diluted with Milli-Q<sup>TM</sup> to a salinity of 34  
11  $\text{g kg}^{-1}$ . A detailed description of the mesocosms is given in (Peperzak et al., 2011).

12 Temperature during *Phaeocystis* growth was kept at 15°C. Irradiance was provided in a semi-  
13 sinusoidal light dark (16:8 h) cycle with a maximum surface PAR of 41  $\text{W m}^{-2}$  in mesocosm 1  
14 and 45  $\text{W m}^{-2}$  in mesocosm 2. Turbulence of the water was provided by pumping surface  
15 water to the bottom of the mesocosm at a turn-over rate of 1  $\text{h}^{-1}$ . The water was enriched with  
16 macronutrients to: 30  $\mu\text{M}$   $\text{NO}_3^-$ , 6.3  $\mu\text{M}$   $\text{PO}_4^{3-}$ , and trace metals and vitamin B1 (Peperzak et  
17 al., 2011). On day 8 of the experiment, when cells were in stationary growth phase, mesocosm  
18 1 received enrichment with the initial nutrient concentrations to examine the effect of  
19 alleviation of nitrogen limitation on the physiological and optical properties of *Phaeocystis*.

20

### 21 **2.2 Sampling**

22 Water samples were taken in the middle of the light period (13:00 h, CET) to measure  
23 salinity, pH, cell abundance, dissolved inorganic nitrogen (DIN), soluble reactive phosphorus

1 (SRP), HPLC pigments including chlorophyll-a (Chl-a), chlorophyll-c2 and -c3 (summed as  
2 Chl-c) and carotenoids, particulate organic carbon (POC) and nitrogen (PON) and PAM  
3 (Walz, Water PAM<sup>TM</sup>) derived Photosystem II quantum efficiency (Fv/Fm) on dark (>20  
4 minutes) adapted samples. A detailed description of the analyses is provided elsewhere  
5 (Peperzak et al., 2011). See Table 1 for a list of measured and derived variables.

6 Surface irradiance ( $\text{W m}^{-2} \text{ nm}^{-1}$ ), used to convert radiance ( $\text{W m}^{-2} \text{ nm}^{-1} \text{ sr}^{-1}$ ) to reflectance ( $R$ ,  
7  $\text{sr}^{-1}$ ), was measured prior to and after the experiment. In addition, phytoplankton absorption  
8 was measured daily at 13:00 h using a 0.55 L integrating cavity absorption meter or ICAM (a-  
9 sphere<sup>TM</sup>, HobiLabs, Tucson, AZ, USA). ICAM-absorption data ( $a_{\text{ph}}$ ,  $\text{m}^{-1}$ ) were blank-  
10 corrected daily by subtracting the absorption of filtered seawater, then divided by chlorophyll-  
11 a or -c concentrations to obtain the chlorophyll-specific absorption coefficients ( $a^*_{\text{Chl}}$ ,  $\text{m}^2$  ( $\text{mg}$   
12 chlorophyll) $^{-1}$ ) in both the exponential and the stationary *Phaeocystis* growth phase.  
13 *Phaeocystis* spectra of  $a^*_{\text{Chl}}$ , together with reflectance data, were used to determine the  
14 appropriate wavelengths in algorithms for the estimation of chlorophyll-a (-c) absorption from  
15 reflectance spectra. Details of the ICAM-absorption, irradiance and radiance measurements  
16 are provided elsewhere (Peperzak et al., 2011).

17

## 18 **2.3 Mesocosms, absorption and fluorescence algorithms**

19 The mesocosm description and analysis of the spectra and is based on the methodological  
20 paper of Peperzak et al. (2011) that contains an extensive description of the experiment,  
21 measurements and validation of the analysis of the absorption and fluorescence signals. The  
22 mesocosm tank, height 0.75 m, diameter 0.5 m and water volume 0.14  $\text{m}^3$  was made of black  
23 high density polyethylene and mounted in a black metal frame made of 30 mm square  
24 aluminum painted black (Fig. 1). To avoid light reflection from the walls the interior of the

1 tank was sand-blasted. The contents was mixed by pumping water at a turn-over rate of  $1\text{ h}^{-1}$   
2 from 0.05 m below the water surface (-0.05 m) to 0.10 m above the bottom (-0.65 m). A total  
3 of 25 Solux™ MR16 halogen 4700K “daylight” lamps of 50 W with a 24° beam spread were  
4 used in a 5 x 5 matrix in a black-painted box that was mounted in a frame at 0.70 m above the  
5 water surface. A variable light:dark cycle with a semi-sinusoidal illumination was made  
6 possible by timers controlling all lamps.

7 Prior and after the experiments of two weeks, surface irradiance ( $E_0$ ) was measured every 15  
8 minutes for at least 24 h from 320-950 nm in 190 channels ( $\text{W m}^{-2} \text{ nm}^{-1}$ ) with a TriOS™  
9 RAMSES-ACC-VIS hyperspectral cosine irradiance sensor (TriOS, GmbH, Oldenburg,  
10 Germany) that was placed in the center of the mesocosm at the position of the water surface.  
11 During experiments the irradiance at the bottom ( $E_b$ ) of the mesocosm (Fig. 1) was measured  
12 every 15 minutes with a similar TriOS™ hyperspectral cosine irradiance sensor. Water  
13 leaving radiance ( $L_w$ ) was measured every 15 minutes with a TriOS™ RAMSES-ACC-VIS  
14 hyperspectral radiance sensor (radiometer, 320-950 nm in 190 channels,  $\text{W m}^{-2} \text{ nm}^{-1} \text{ sr}^{-1}$ ) at an  
15 angle of 50° nadir at 0.08 m above the water surface (Fig. 1). An integrating cavity  
16 absorption meter or ICAM (a-sphere spectrophotometer, HOBI Labs™, Tucson, AZ, USA)  
17 was used as an independent method to measure sample absorption ( $\text{m}^{-1}$ ). This type of  
18 instrument is very accurate, also at low concentrations, without interference by particle  
19 scattering.

20 Based on the averaged spectra from the middle of the light period (13:00-14:00 h), four  
21 optical properties were derived: 1-the total number of photons absorbed by phytoplankton, 2-  
22 the total number of photons emitted by fluorescence, 3,4- the Chlorophyll-c and Chlorophyll-  
23 a concentration, respectively. The fifth quantity, the phytoplankton quantum efficiency ( $\phi_{\text{ph}}$ ) is  
24 defined as the ratio of mol photons emitted as fluorescence divided by the mol photons  
25 absorbed by the pigments and is therefore the ratio of property 2 over 1.

1 1- From a comparison of the irradiance sensor at the bottom of each mesocosm with  
2 the known irradiance at the water surface, the wavelength-dependent attenuation in the  
3 mesocosm was derived. This attenuation was corrected for the (small) effects of pure water  
4 and scattering effects at the mesocosm wall and the total number of absorbed photons was  
5 calculated as the absorption times the illumination at each wavelength and integrated over the  
6 interval 400-672 nm. The stricter upper limit of 672 nm to the Potential Fluorescence  
7 Radiation (PFR), is based on a central fluorescence emission at 682 nm and a Stokes shift of  
8 10 nm that determined the minimum extra energy needed for the excitation of a chlorophyll  
9 molecule. The typical available PFR just below the water surface is  $138 \mu\text{mol photons m}^{-2} \text{ s}^{-1}$   
10 (mesocosm 1) and slightly higher for mesocosm 2 ( $151 \mu\text{mol photons m}^{-2} \text{ s}^{-1}$ ).

11 2- The classic Fluorescence Line Height (FLH) algorithm (Abbott and Letelier, 1999) was  
12 applied on the remote sensing reflectance spectra (R), calculated as the ratio of the radiance  
13 spectra collected above water (Sr Fig. 1) divided by the illumination irradiance.

14 
$$\text{FLH} = R_{\text{max}} - R_{\text{base}} \quad (\text{sr}^{-1}) \quad (1\text{a})$$

15 with 
$$R_{\text{base}} = R_{b1} + (\lambda_{\text{max}} - \lambda_{b1}) * ((R_{b1} - R_{b2}) / (\lambda_{b1} - \lambda_{b2})) \quad (\text{sr}^{-1}) \quad (1\text{b})$$

16  $R_{\text{max}}$  is at the fluorescence peak ( $\lambda = 682 \text{ nm}$ ) in the mesocosm reflectance spectra,  $R_{\text{base}}$  is the  
17 baseline reflectance value at  $R_{\text{max}}$ , calculated linearly from the reflectance between  $R_{b1}$  and  
18  $R_{b2}$  with  $b_1=650 \text{ nm}$  and  $b_2=710 \text{ nm}$ . In order to derive the number of emitted photons in the  
19 mesocosm, the FLH was first multiplied by the irradiance spectrum to obtain a baseline  
20 corrected radiance above water at  $682 \text{ nm}$  ( $\text{W m}^{-2} \text{ nm}^{-1} \text{ sr}^{-1}$ ). Then the signal was converted to  
21 photons and integrated over  $4\pi \text{ sr}$  (assuming isotropic emission) and integrated over the  
22 spectral range (650-710 nm), assuming a Gaussian distribution with a FWHM of 25 nm.  
23 Subsequently, the emission was corrected for the water-air transition and the internal  
24 absorption in the mesocosm before it reaches the radiance sensor by water, ( $0.43 \text{ m}^{-1}$  at 682

1 nm) and self-absorption by the phytoplankton (Huot et al., 2005). We refer to the publication  
2 of (Peperzak et al., 2011) for a more extensive description and validation of this conversion.

3 3- The Chlorophyll-c concentration was calculated from reflectance (R) by a 4-wavelength (at  
4  $\lambda = 450, 466, 480$  and 700 nm) absorption algorithm (ARP-4 $\lambda_{Chl-c}$ ) that was developed and  
5 positively applied by (Astoreca et al., 2009) to detect *Phaeocystis* in the North Sea:

6  $a_{Chl-c} = a_{w,700} \times R_{700} \times (1/R_{466} - (1/R_{450})^{(1-w)} \times (1/R_{480})^w) \text{ (m}^{-1}\text{)} \quad (2a)$

7 With the absorption by pure water:

8  $a_{w,700} = 0.572 \text{ m}^{-1} (15^\circ\text{C}) \quad (\text{Buiteveld et al., 1994}) \quad (2b)$

9 and the weight (w) is determined by the position of the Chl-c absorption maximum (466 nm)  
10 relative to the two reference (baseline) wavelengths (450 and 480 nm):

11  $w = (\lambda_{466, Chlc} - \lambda_{450}) / (\lambda_{480} - \lambda_{450}) = 0.53 \quad (2c)$

12 4- A comparable absorption algorithm (ARP-4 $\lambda_{Chla}$ ) for Chlorophyll-a was derived after  
13 choosing the appropriate wavelengths, including the Chl-a absorption maximum (438 nm):

14  $a_{Chl-a} = a_{w,700} \times R_{700} \times (1/R_{438} - (1/R_{425})^{(1-w)} \times (1/R_{450})^w) \text{ (m}^{-1}\text{)} \quad (3a)$

15 With water absorption given by eq. (1b) and the weight (w) by:

16  $w = (\lambda_{438, Chla} - \lambda_{425}) / (\lambda_{450} - \lambda_{425}) = 0.52 \quad (3b)$

17

18

19

1    **2.4 Statistics**

2    To test the null hypothesis that there is no difference between means of variables measured in  
3    the two mesocosms, two-sample t-tests were performed in SYSTAT™ version 12. Linear  
4    regression equations were calculated in SYSTAT™ or Excel™ 2003. 95% confidence  
5    intervals ( $\pm 95\% \text{ c.i.}$ ) around a variable mean  $m$  were calculated from a t-distribution using  $n$   
6    observations (days),  $n-1$  degrees of freedom and the standard deviation of the mean  $sd$  as:  $m \pm$   
7     $95\% \text{ c.i.} = m \pm t(0.05; n-1) \times sd / \sqrt{n}$ . The standard error ( $= sd / \sqrt{n}$ ) provided in linear  
8    regression by SYSTAT™ was used to calculate 95% confidence intervals of regression  
9    slopes.

10

11    **3. Results**

12    **3.1 Phytoplankton dynamics (ex situ observations)**

13    Inoculation of the mesocosms was followed by a three day exponential increase in  
14    *Phaeocystis* cell abundance, Chl-a, Chl-c, POC and PON concentrations (Figs. 2A, C-F).  
15    Compared to mesocosm 1, the higher surface irradiance in mesocosm 2 led to 17% more cells  
16    on day 5, when the stationary growth phase was reached in both mesocosms due to nitrogen  
17    limitation (Fig. 2B). In both mesocosms, cell abundances in stationary growth phase  
18    decreased with an average rate of  $-0.07 \text{ d}^{-1}$ . The 30  $\mu\text{M}$  nitrate in the nutrient-spike added to  
19    mesocosm 1 on day 8, was already depleted by *Phaeocystis* on day 9 (Fig. 2B) and  
20    incorporated as PON (Fig. 2F). In addition, *Phaeocystis* cells, Chl-a and Chl-c concentrations  
21    increased after the nutrient-spike (Figs. 2A, C-D). In a separate experiment (no data shown),  
22    in which a mesocosm 2 water sample on day 10 was spiked with only nitrate, the resumption  
23    of cell growth and an increase in Fv/Fm confirmed that nitrogen was the limiting element.

1    **3.2 Physiology and pigment composition (ex situ observations)**

2    After the depletion of DIN on day 4, Fv/Fm declined in both mesocosms (Fig. 3A), while the  
3    C:Chl ratios increased (Fig. 3C). The nutrient-spike on day 8 in mesocosm 1 caused a  
4    temporary increase in Fv/Fm (Fig. 3A) and led to significantly lower C:N ( $t = -25.2$ ,  $df = 5$ ,  $p$   
5     $< 0.001$ ) and C:Chl ratios ( $t = -8.5$ ,  $df = 5$ ,  $p < 0.001$ ) in mesocosm 1 relative to mesocosm 2  
6    (Figs. 3B, C). The difference in Carotenoids: Chl between mesocosm 1 and 2 (Fig. 3D) from  
7    day 9 onwards was also significant ( $t = -6.8$ ,  $df = 5$ ,  $p < 0.01$ ). Thus, the nutrient-spike on day  
8    8 caused a shift in Fv/Fm, C:N, C:Chl and Carotenoids: Chl (Figs. 3A, B - D).

9

10    **3.3 Absorption and fluorescence (optical observations)**

11    **3.3.1 ICAM absorption**

12    The ICAM absorption spectra of mesocosm water samples contained three major peaks: at  
13    438 nm (Chl-a), 466 nm (Chl-c) and 674 nm (Chl-a). In the exponential growth phase,  $a^*_{Chl}$   
14    was lower than in the stationary growth phase, due to the increase in Carotenoids after  
15    nitrogen was depleted (Fig. 3D). These differences in  $a^*_{Chl}$  between exponential and  
16    stationary growth phase were significant at 438 and 466 nm, but not at 674 nm (Table 2).

17    **3.3.2 Reflectance absorption**

18    The specific chlorophyll-a and -c absorption ( $a_{Chl-a}$  and  $a_{Chl-c}$ ) computed from reflectance  
19    spectra (Figs. 4A-B) closely resembled the development of *Phaeocystis* cell abundance and  
20    Chl-a and -c concentrations (Figs. 2A, C-D). In both mesocosms, total Chl absorption,  $a_{Chl-a}(-$   
21     $c)$  correlated well with HPLC-measured Chl-a and Chl-c concentrations (Figs. 4C-D) and the  
22    regression slopes of the two variables in the mesocosms were not significantly different  
23    (Table 3). When the data of both mesocosms were split by growth phase, the exponential

1 phase (day 1 to 4) regression equations accurately (both  $r^2 = 0.98$ ) estimated both Chl-a and  
2 Chl-c (Figs. 4E-F). The stationary phase (day 5 to 14) regression intercepts between  $a_{Chl-a(-c)}$   
3 and Chl-a and Chl-c concentrations were lower than in exponential growth phase (Figs. 4E-F),  
4 although not significantly (Table 3). This means that application of the regression equations  
5 combining both growth phases (Table 3), will lead to small underestimations of Chl-a and  
6 Chl-c concentrations in the exponential growth phase, and small overestimations of Chl-a and  
7 Chl-c concentrations in the stationary phase (Figs. 4 E-F).

8 **3.3.3 Fluorescence**

9 Fluorescence emission estimated from the water leaving radiance (Fig. 5A) resembled  
10 *Phaeocystis* cell dynamics (Fig. 2A) and was well correlated with Chl-a (Fig. 5B; overall  $r^2 =$   
11 0.81, Table 4). When the data of both mesocosms was split by growth phase, the stationary  
12 phase (day 5 to 14) regression slope and intercept were significantly different from those in  
13 exponential phase (day 1 to 4) (Fig. 5C, Table 4). This means that according to expectation,  
14 nutrient-stressed cells in stationary growth phase have higher fluorescence intensity per unit  
15 chlorophyll.

16 **3.4 Fluorescence quantum efficiency (optical observations)**

17 The fluorescence efficiency ( $\phi_{ph}$ ) calculated as mol photons emitted as fluorescence divided  
18 by the mol photons absorbed by the phytoplankton pigments increased during exponential  
19 growth, stabilized from day 5 to 8 and then decreased (Fig. 6). No apparent change in  $\phi_{ph}$  was  
20 observed in response to the nutrient-spike on day 8 to mesocosm 1.

21 **3.5 Carbon growth rate and proxy comparison**

22 In order to relate dynamics in light absorption and fluorescence to *Phaeocystis* physiology in  
23 the different growth phases, the dynamics of carbon growth rate ( $\mu_{POC}$ ) was compared to

1 Fv/Fm, C:Chl and  $\phi_{ph}$  (Figs. 7A-C). Because the cellular Chl-c content of *Phaeocystis* is  
2 about the same as the cellular Chl-a content (Figs. 4C,D) and total chlorophyll (Chl) was  
3 linearly correlated to Chl-a ( $Chl = 2.28 \times Chl-a$ ,  $r^2 = 0.99$ ), C:Chl was used rather than C:Chl-  
4 a and C:Chl-c separately.

5 The proxy comparison showed hyperbolic relations of  $\mu_{POC}$  with C: Chl and Fv/Fm with  
6 highly variable values at  $\mu_{POC} \sim 0.0 \text{ d}^{-1}$  (Figs. 7A-B). As could be expected from Figs. 7A and  
7 B, Fv/Fm was inversely linearly correlated to C:Chl ( $r^2 = 0.88$ ). The good correlation implies  
8 that under the present experimental conditions Fv/Fm and C:Chl, as measured either in water  
9 samples or derived from water-leaving radiance are directly comparable physiological  
10 proxies.

11 Fluorescence quantum efficiency did not show any correlation with growth rate (Fig. 7C). It  
12 appears that in both mesocosms  $\phi_{ph}$  is a poor proxy for *Phaeocystis* carbon production in both  
13 mesocosms.

14

#### 15 **4. Discussion**

16 The aim of the mesocosm experiments was to investigate a relation between optical remote  
17 sensing and “standard” oceanographic measurements of phytoplankton physiology during  
18 different growth phases (here: nitrogen-controlled growth) of *Phaeocystis* and to infer  
19 possible implications for estimates of primary productivity. The standard physiological and  
20 reflectance measurements, in combination with the effect of a nutrient-spike to one  
21 mesocosm, proved that growth of *Phaeocystis* was indeed nitrogen-limited during the  
22 experiments. By measuring the in situ fluorescence (F) increase due to nitrogen limitation,  
23 and the increase in photons absorbed by phytoplankton (PFR), an optical estimate of the  
24 quantum efficiency of fluorescence  $\phi_{ph}$  (= F/PFR) could be made. It is shown that of the

1 physiological diagnostics neither  $\phi_{ph}$ , nor Photosystem II quantum efficiency (Fv/Fm) nor  
2 C:Chl are reliable estimators of *Phaeocystis* growth rates. This may have consequences for  
3 global carbon fixation estimates using remote sensing data assessing phytoplankton  
4 physiology.

5 **4.1 Phytoplankton dynamics**

6 Temperature, salinity, irradiance and pH were at or near values for optimum *Phaeocystis*  
7 growth (Peperzak, 2002). Exponential phase growth rate ( $\mu = 0.7 \text{ d}^{-1}$ ) and stationary phase  
8 mortality rate ( $d = -0.07 \text{ d}^{-1}$ ) were equal to the rates obtained in cultures of *P. globosa* strain  
9 Ph91 (Peperzak et al., 2000a;Peperzak et al., 2000b). The carbon and photopigment contents  
10 of *Phaeocystis* in the mesocosms were comparable to published values, although cellular Chl-  
11 a and Chl-c content were relatively low (Table 5). On the other hand, the fucoxanthin to Chl-a  
12 ratio was high which is probably caused by 1) an adaptation to the low irradiance environment  
13 where this flagellate can thrive (Peperzak, 1993;Seoane et al., 2009) and/or 2) the effect of  
14 nitrogen-limited growth on the Carotenoids: Chl ratio (Fig. 3D). In mesocosm 2 *Phaeocystis*  
15 in stationary phase reached a C:N of 20, which is equal to the subsistence quota of 0.05 mol N  
16 mol C<sup>-1</sup> in diatoms (Edwards et al., 2003). The rapid depletion of nitrate during the initial days  
17 of the experiment and the constant increase in C:N, combined with the decrease in C:N,  
18 resumption of cell growth and increase in Fv/Fm after the nutrient-spike, convincingly  
19 showed that *Phaeocystis* was nitrogen-limited in the stationary phase.

20 The physiological indicator Fv/Fm declined when nitrogen had been depleted on day 4. In  
21 addition, C:Chl increased. Both indicators responded directly following the nutrient-spike to  
22 the nitrogen-depleted *Phaeocystis* on day 8. C:Chl was inversely linearly correlated with  
23 Fv/Fm, but carbon growth rate was not. This can be explained by the fact that both Fv/Fm and  
24 C:Chl declined continuously after nitrogen depletion while cell division immediately halted

1 on day 5. As a consequence, Fv/Fm and C:Chl not only signal physiological change, they are  
2 also indicative of the persistence of nitrogen depletion in *Phaeocystis*. A comparable  
3 conclusion was reached for the decline of Fv/Fm and the duration of nitrogen depletion in the  
4 diatom *Thalassiosira pseudonana* (Parkhill et al., 2001). On the other hand, under balanced  
5 growth conditions, i.e. steady-state nitrogen-limited growth, the value of Fv/Fm in *T.*  
6 *pseudonana* was high and comparable to the value in nutrient-replete cultures (Parkhill et al.,  
7 2001). In other words, the steady 10 day change after an abrupt nitrogen depletion make that  
8 Fv/Fm and C:Chl are not good indicators of short-term nutrient-limited phytoplankton growth  
9 rates.

10 In the early stationary phase (day 4-8), the 10% lower surface irradiance in mesocosm 1 led to  
11 a slightly lower ( $94 \pm 21$ ) but not significantly different C:Chl than in mesocosm 2 ( $106 \pm 28$ ).  
12 Comparable minor effects on cellular chlorophyll contents have been measured in *Phaeocystis*  
13 cultured at 10 and 100  $\mu\text{mol}$  photons  $\text{m}^{-2} \text{ s}^{-1}$  (Astoreca et al., 2009). The reduction of water  
14 column irradiance due to self-shading by increased chlorophyll concentrations during  
15 exponential growth would, therefore, have little effect on C:Chl. Far more important than the  
16 (relatively weak) effect of irradiance on C:Chl was the factor 10 variability in C:Chl when  
17 *Phaeocystis* went from the exponential ( $\text{C:Chl} = 30$ ) to the late stationary growth phase  
18 ( $\text{C:Chl} = 200$ , Fig. 3C and Table 5). This variability confirms that chlorophyll concentration is  
19 not a reliable indicator of phytoplankton biomass (Behrenfeld et al., 2009; Kruskopf and  
20 Flynn, 2006), which has implications for the correct conversion of chlorophyll to carbon in  
21 chlorophyll-based primary production models (Cloern et al., 1995; Sathyendranath et al.,  
22 2009).

23 **4.2 Pigments and absorption**

1 Nitrogen depletion led to increases in Carotenoids concentrations relative to chlorophyll.  
2 Comparable increases in light absorption under nitrogen limitation, due to increased  
3 Carotenoid: Chl-a ratios, have been observed in other phytoplankton species (Heath et al.,  
4 1990; Staehr et al., 2002). The increase of Carotenoids to Chl ratio had a direct effect on the  
5 estimation of light absorption from the reflection spectra and ICAM measurements. The  
6 excellent correlations (Table 3) between  $a_{Chl-a}$  and  $a_{Chl-c}$  and respectively Chl-a and Chl-c  
7 concentrations in exponential phase (both  $r^2 = 0.98$ ) were lower in stationary phase ( $0.59 < r^2$   
8  $< 0.82$ ). Besides more variability in stationary phase,  $a_{Chl}$  was lower than in exponential phase  
9 due to interference by Carotenoids in the reflection spectrum. This interference was more  
10 pronounced for  $a_{Chl-c}$  than for the  $a_{Chl-a}$  (Table 3), because the  $a_{Chl-c}$  algorithm employs  
11 wavelengths from 450 to 480 nm where Carotenoids absorption is more pronounced (Fujiki  
12 and Taguchi, 2002; Lubac et al., 2008).

13 The interference of Carotenoids in stationary phase will increase when total pigment  
14 absorption ( $a_{ph}$ ) will be measured instead of specific chlorophyll absorption. It is not  
15 surprising, therefore, that by using the ICAM data (400 to 672 nm) the correlation of  
16 absorption with Chl was lower ( $r^2 = 0.74$ ) than when using the Chl-a and Chl-c specific  
17 algorithms. Carotenoids interference in stationary phase also explains the limited apparent  
18 linearity of chlorophyll detection by ICAM absorption to a maximum of approximately 50  $\mu g$   
19  $L^{-1}$  (Peperzak et al., 2011). At a high nitrogen-limited *Phaeocystis* biomass, the use of total  
20 absorption including the Carotenoids, leads to an overestimation of the chlorophyll  
21 concentration.

## 22 **4.3 Fluorescence quantum efficiency**

23 The optically measured fluorescence signal correlated well with the *ex situ* measured Chl-a  
24 concentrations and, as expected, showed a relative fluorescence increase in stationary phase.

1  $\varphi_{ph}$  in mesocosm 2 ranged by more than 100%, from  $\approx 0.8$  to  $\approx 1.7\%$  (Fig. 6). Satellite  
2 estimates of  $\varphi_{ph}$  have a corresponding range, 0 – 3% (Huot et al., 2005; Behrenfeld et al.,  
3 2009). However, there was no correlation with  $\mu$  (cell growth rate) or  $\mu_{POC}$  (carbon growth  
4 rate, Fig. 7C), due to the effect of changing Carotenoids: Chl ratio as a result of nitrogen  
5 limitation. This suggests that in order to relate growth conditions and fluorescence signal  
6 strength, new optical proxies should be developed for the photon absorption and emission by  
7 individual pigments (Fawley, 1989).

8 Even though  $\varphi_{ph}$  can be estimated using appropriate fluorescence and absorbance algorithms,  
9 its value will not be a reliable indicator of actual nitrogen-controlled *Phaeocystis* growth rate.  
10  $\varphi_{ph}$  is also a diagnostic for the duration of nitrogen depletion in *Phaeocystis*, which adds to the  
11 discussion on the physiological significance of Fv/Fm and C:Chl. For instance, under steady-  
12 state nitrogen-limited growth, the value of Fv/Fm in *T. pseudonana* is as high as the value in  
13 nutrient-replete cultures (Parkhill et al., 2001). As the present investigation was deemed to be  
14 exemplary of the phytoplankton dynamics during the wax and wane of a short-term bloom,  
15 i.e. a fast reduction from a high concentration of the limiting nutrient towards depletion, a  
16 real-world estimate of  $\varphi_{ph}$  might behave similar as  $\varphi_{ph}$  in the mesocosms.

17 On the other hand, in oceanic waters the supply of the limiting nutrient may be low but  
18 relatively more constant, such as by aeolian deposition of iron or by continuous heterotrophic  
19 remineralization of organic material in the water column. For iron-limited phytoplankton  
20 growth,  $\varphi_{ph}$  derived from satellite data was elevated (Behrenfeld et al., 2009), so in 82% of the  
21 oceanic regions with a low iron deposition rate,  $\varphi_{ph}$  appears to be a reliable remote sensing  
22 physiology proxy. This applicability of  $\varphi_{ph}$  corresponds with that of Fv/Fm as a good  
23 physiological proxy in iron-limitation studies (Timmermans et al., 2001; Timmermans et al.,  
24 2008). Maybe Fe-limitation has a more pronounced effect on  $\varphi_{ph}$  than limitation of the major  
25 nutrients (N, P).

1 The present *Phaeocystis* study is an example of how experiments can contribute to validate  
2 assumptions on optical data that are being made in the estimation of global carbon production.  
3 More experimental data is needed from phytoplankton species that differ in their pigment  
4 composition and in the effects of short- and long-term nutrient (N, P, Fe) limitation so that  
5 new optical proxies for phytoplankton physiology can be examined. Until these issues have  
6 been resolved we should be aware of the obscured view of phytoplankton physiology, hence  
7 marine primary production estimates using remote sensing.

8

## 9 **Acknowledgements**

10 We gratefully acknowledge the help of the following NIOZ personnel. S. Oosterhuis  
11 performed HPLC photo-pigment analyses. POC and PON were analyzed by S. Crawford.  
12 Nutrients were analyzed by K. Bakker, E. van Weerlee and J. van Ooijen. B. Hoogland (Van  
13 Hall Larenstein college, Leeuwarden, The Netherlands) assisted in sampling and sample  
14 analysis. We acknowledge the useful comments of Anita Buma (U. Groningen, The  
15 Netherlands) on an earlier version of the ms. H.J.v.d.W was supported by the BSIK Climate  
16 Changes Spatial Planning A6 project. Financial support for this research was obtained from  
17 NWO project EO-078: 'Improved quantification of Southern Ocean diatoms as indicators for  
18 Carbon fixation', granted to H.J.v.d.W.

19

20

## 21 **References**

22 Abbott, M. R., and Letelier, R. M.: Algorithm theoretical basis document chlorophyll  
23 fluorescence (MODIS product number 20), NASA, 1999.

1 Astoreca, R., Rousseau, V., Ruddick, K., Knechciak, C., van Mol, B., Parent, J.-Y., and  
2 Lancelot, C.: Development and application of an algorithm for detecting *Phaeocystis globosa*  
3 blooms in the Case 2 Southern North Sea waters, J. Plankton Res., 31, 287-300, 2009.

4 Behrenfeld, M. J., Boss, E., Siegel, D. A., and Shea, D. M.: Carbon-based ocean productivity  
5 and phytoplankton physiology from space, Glob. Biochem. Cycles, 19, GB1006, doi:  
6 10.1029/2004GB002299, 2005.

7 Behrenfeld, M. J., Westberry, T. K., Boss, E. S., O'Malley, R. T., Siegel, D. A., Wiggert, J.  
8 Fransz, B. A., McClain, C. R., Feldman, G. C., Doney, S. C., Moore, J. K., Dall'Olmo, A.  
9 Milligan, A. J., Lima, I., and Mahowald, N.: Satellite-detected fluorescence reveals global  
10 physiology of ocean phytoplankton, Biogeosciences, 6, 779-794, 2009.

11 Buiteveld, H., Hakvoort, J. M. H., and Donze, M.: The optical properties of pure water, Ocean  
12 Optics XII, 1994, 174-183,

13 Buma, A. G. J., Bano, N., Veldhuis, M. J. W., and Kraay, G. W.: Comparison of the  
14 pigmentation of two strains of the prymnesiophyte *Phaeocystis* sp, Neth. J. Sea Res., 27, 173-  
15 182, 1991.

16 Carder, K. L., Chen, R., and Hawes, S.: Algorithm theoretical basis document: Instantaneous  
17 photosynthetically available radiation and absorbed radiation by phytoplankton. Version 7,  
18 NASA, 24, 2003.

19 Cloern, J. E., Grenz, C., and Vidergar-Lucas, L.: An empirical model of the phytoplankton  
20 chlorophyll:carbon ratio-the conversion factor between productivity and growth rate, Limnol  
21 Oceanogr, 40, 1313-1321, 1995.

22 Cullen, J., and Lewis, A. G.: Biological processes and optical measurements near the sea  
23 surface: Some issues relevant to remote sensing, J. Geoph. Res., 100, 13,255-213,266, 1995.

24 DiTullio, G. R., Grebmeier, J. M., Arrigo, K. R., Lizotte, M. P., Robinson, D. H., Leventer,  
25 A., Barry, J. P., VanWoert, M. L., and Dunbar, R. B.: Rapid and early export of *Phaeocystis*  
26 *antarctica* blooms in the Ross Sea, Antarctica, Nature, 404, 595-598, 2000.

1 Edwards, V. R., Tett, P., and Jones, K. J.: Changes in the yield of chlorophyll a from  
2 dissolved available inorganic nitrogen after an enrichment event - applications for predicting  
3 eutrophication in coastal waters, *Continental Shelf Research* 23, 1771-1785, 2003.

4 Falkowski, P., Greene, R. M., and Geider, R.: Physiological limitations on phytoplankton  
5 productivity in the ocean, *Oceanogr. Mar. Biol.*, 5, 84-91, 1992.

6 Falkowski, P., and Kolber, Z.: Variations in Chlorophyll Fluorescence Yields in  
7 Phytoplankton in the World Oceans, *Aust. J. Plant Physiol.*, 22, 341-355, 1995.

8 Falkowski, P. G., Dubinsky, Z., and Wyman, K.: Growth-irradiance relationships in  
9 phytoplankton, *Limnol Oceanogr*, 30, 311-321, 1985.

10 Fawley, M. W.: A new form of chlorophyll *c* involved in light-harvesting, *Plant. Physiol.*, 91,  
11 727-732, 1989.

12 Field, C. B., Behrenfeld, M. J., Randerson, J. T., and Falkowski, P.: Primary production of the  
13 biosphere: integrating terrestrial and oceanic components, *Science*, 281, 237-240, 1998.

14 Fujiki, T., and Taguchi, S.: Variability in chlorophyll *a* specific absorption coefficient in  
15 marine phytoplankton as a function of cell size and irradiance, *J. Plankton Res.*, 24, 859-874,  
16 2002.

17 Heath, M. R., Richardson, K., and Kiørboe, T.: Optical assessment of phytoplankton nutrient  
18 depletion, *Journal of Plankton Research*, 12, 381-396, 1990.

19 Huot, Y., Brown, C. A., and Cullen, J. J.: New algorithms for MODIS sun-induced  
20 chlorophyll fluorescence and a comparison with present data products, *Limnol. Oceanogr.*:  
21 *Methods*, 3, 108-130, 2005.

22 Huot, Y., Franz, B. A., and Fradette, M.: Estimating variability in the quantum yield of Sun-  
23 induced chlorophyll fluorescence: A global analysis of oceanic waters, *Remote Sensing*  
24 *Environment*, 132, 238-253, 2013.

25 Kiefer, D. A.: Chlorophyll a fluorescence in marine centric diatoms: Responses of  
26 chloroplasts to light and nutrient stress, *Marine Biology*, 23, 39-46, 1973.

1 Kromkamp, J., and Foster, R. M.: The use of variable fluorescence measurements in aquatic  
2 ecosystems: differences between multiple and single turnover measuring protocols and  
3 suggested terminology, European Journal of Phycology, 38, 103-112, 2003.

4 Kruskopf, M., and Flynn, K. J.: Chlorophyll content and fluorescence responses cannot be  
5 used to gauge reliably phytoplankton biomass, nutrient status or growth rate, New Phytol,  
6 169, 525-536, 2006.

7 Kurekin, A. A., Miller, P.I., Van der Woerd, H.J.: Satellite discrimination of Karenia  
8 mikimotoi and Phaeocystis harmful algal blooms in European coastal waters: Merged  
9 classification of ocean colour data, Harmful Algae, 31, 163-176,  
10 doi:10.1016/j.hal.2013.11.003, 2014.

11 Lubac, B., Loisel, H., Guiselin, N., Astoreca, R., Artigas, L. F., and Meriaux, X.:  
12 Hyperspectral and multispectral ocean color inversions to detect *Phaeocystis globosa* blooms  
13 in coastal waters, J. Geophys. Res., 113, C06026, doi: 06010.01029/02007JC004451, 2008.

14 Ly, J., Philippart, C. J. M., and Kromkamp, J.: Phosphorus limitation during a phytoplankton  
15 spring bloom in the western Dutch Wadden Sea, J. Sea Res., 88, 109-120,  
16 <http://dx.doi.org/10.1016/j.seares.2013.12.010>, 2014.

17 Martinez-Vicente, V., Dall'Olmo, G., Tarran, G., Boss, E., and Sathyendranath, S.: Optical  
18 backscattering is correlated with phytoplankton carbon across the Atlantic Ocean,  
19 Geophysical Research Letters, 40, 1154-1158, 10.1002/grl.50252, 2013.

20 Parkhill, J.-P., Maillet, G., and Cullen, J. J.: Fluorescence-based maximal quantum yield for  
21 PSII as a diagnostic of nutrient stress, J. Phycol. , 37, 517-529, 2001.

22 Peperzak, L.: Daily irradiance governs growth rate and colony formation of Phaeocystis  
23 (Prymnesiophyceae), J. Plankton Res., 15, 809-821, 1993.

24 Peperzak, L., Duin, R. N. M., Colijn, F., and Gieskes, W. W. C.: Growth and mortality of  
25 flagellates and non-flagellate cells of Phaeocystis globosa (Prymnesiophyceae), J. Plankton  
26 Res., 22, 107-120, 10.1093/plankt/22.1.107, 2000a.

1 Peperzak, L., Gieskes, W. W. C., Duin, R. N. M., and Colijn, F.: The vitamin B requirement  
2 of *Phaeocystis globosa* (Prymnesiophyceae), Journal of Plankton Research, 22, 1529-1537,  
3 2000b.

4 Peperzak, L.: The wax and wane of *Phaeocystis globosa* blooms, Rijksuniversiteit Groningen,  
5 The Netherlands, Groningen, 254 pp., 2002.

6 Peperzak, L., Timmermans, K. R., Wernand, M. R., Oosterhuis, S., and Van der Woerd, H. J.:  
7 A mesocosm tool to optically study phytoplankton dynamics, Limnol. Oceanogr.: Methods, 9,  
8 232-244, 2011.

9 Rousseau, V., Mathot, S., and Lancelot, C.: Calculating carbon biomass of *Phaeocystis* sp.  
10 from microscopic observations, Marine Biology, 107, 305-314, 1990.

11 Saba, V. S., and al., e.: Challenges of modeling depth-integrated marine primary productivity  
12 over multiple decades: A case study at BATS and HOT, Global Biochem Cycles, 24,  
13 doi:10.1029/2009GB003655, 2010.

14 Sathyendranath, S., Stuart, V., Nair, A., Oka, K., Nakane, T., Bouman, H., Forget, M.-H.,  
15 Maass, H., and Platt, T.: Carbon-to-chlorophyll ratio and growth rate of phytoplankton in the  
16 sea, Mar. Ecol. Prog. Ser., 383, 73-84, 2009.

17 Seoane, S., Zapata, M., and Orive, E.: Growth rates and pigment patterns of haptophytes  
18 isolated from estuarine waters, J. Sea Res., 62, 286-294, 2009.

19 Smith, W. O., Codispoti, L. A., Nelson, D. M., Manley, T., Buskey, E. J., Niebauer, H. J., and  
20 Cota, G. F.: Importance of *Phaeocystis* blooms in the high-latitude ocean carbon cycle,  
21 Nature, 352, 514-516, 1991.

22 Staehr, P. A., Henriksen, P., and Markager, S.: Photoacclimation of four marine  
23 phytoplankton species to irradiance and nutrient availability, Mar. Ecol. Prog. Ser., 238, 47-  
24 59, 2002.

25 Timmermans, K. R., Davey, M. S., van der Wagt, B., Snoek, J., Geider, R. J., Veldhuis, M. J.  
26 W., Gerringa, L. J. A., and De Baar, H. J. W.: Co-limitation by iron and light of *Chaeotoceros*  
27 *brevis*, *C. dichaeta* and *C. calcitrans* (Bacillariophyceae), Mar. Ecol. Prog. Ser., 217, 287-  
28 297, 2001.

1 Timmermans, K. R., Veldhuis, M. J. W., Laan, P., and Brussaard, C. P. D.: Probing natural  
2 iron fertilization near the Kerguelen (Southern Ocean) using natural phytoplankton  
3 assemblages and diatom cultures, Deep-Sea-Res. II. , 55, 693-705, 2008.

4 Vogt, M., O'Brien, C., Peloquin, J., Schoemann, V., Breton, E., Estrada, M., Gibson, J.,  
5 Karentz, D., Van Leeuwe, M. A., Stefels, J., Widdicombe, C., and Peperzak, L.: Global  
6 marine plankton functional type biomass distributions: *Phaeocystis* spp., Earth Syst. Sci.  
7 Data, 4, 107-120, 10.5194/essd-4-107-2012, 2012.

8 Wassmann, P., Vernet, M., Mitchell, B. G., and Rey, F.: Mass sedimentation of *Phaeocystis*  
9 *pouchetii* in the Barents Sea, Mar Ecol Prog Ser, 66, 183-195, 1990.

10

1 Table 1. List of used variables, measurements and computations.

Symbol	Description	Measurement or Computation	Units
$a_{ph}$	Phytoplankton (total pigment) absorption coefficient	Integrating cavity absorption meter, from 400 to 672 nm	$m^{-1}$
$a_{Chl-a(-c)}$	Chlorophyll-a or -c absorption coefficient	ARP $(-4\lambda)(-Chl-a/c) 4$ -wavelength algorithm from reflectance spectrum (eq. 2)	$m^{-1}$
$a_{Chl}$	Total chlorophyll absorption coefficient	$a_{Chl-a} + a_{Chl-c}$	$m^{-1}$
$a^*_{Chl-a(-c)}$	Chlorophyll-a or c-specific absorption coefficient	$a_{ph} / Chl-a$ (at 428 or 674 nm) or $a_{ph} / Chl-c$ (at 466 nm) (Table 2)	$m^{-2} (mg Chl)^{-1}$
$C : Chl(-a)$	Carbon to Chlorophyll (-a) ratio	$POC / Chl$ or $POC / Chl-a$	$g g^{-1}$
C:N	Carbon to Nitrogen ratio	$POC / PON$	$mol mol^{-1}$
Carotenoids	Sum of fucoxanthin, diatoxanthin, diadinoxanthin, $\beta, \epsilon$ - and $\beta, \beta$ -carotene	HPLC	$\mu g L^{-1}$
$C : cell$	Carbon content per cell	$POC / N_t$	$pg cell^{-1}$
Carots : Chl	Carotenoids to chlorophyll ratio	$Carots / Chl$	Unitless
Chl-a	Chlorophyll-a	HPLC	$\mu g L^{-1}$
Chl-c	Chlorophyll-c	HPLC	$\mu g L^{-1}$
Chl	Sum of Chl-a and Chl-c	HPLC	$\mu g L^{-1}$
$Chl-a(-c) : cell$	Chl-a (-c) content per cell	$Chl-a(-c) / N_t$	$pg cell^{-1}$
DIN	Dissolved Inorganic Nitrogen	Continuous flow chemistry	$\mu mol L^{-1}$

F	Chlorophyll-a fluorescence	Fluorescence emission	$\mu\text{mol}$ photons $\text{m}^{-2} \text{s}^{-1}$
$F_0$	Dark-adapted chlorophyll fluorescence	Pulse Amplitude Modulation fluorometer	Unitless
$F_v/F_m$	Photosystem II quantum efficiency	Pulse Amplitude Modulation fluorometer	Unitless
$N_{t(t+1)}$	Cell concentration on day $t(t+1)$	Flow cytometer	cells $\mu\text{L}^{-1}$
$N : \text{cell}$	Nitrogen content per cell	$\text{PON} / N_t$	$\text{pg cell}^{-1}$
PFR	Potential Fluorescence Radiation	Irradiance (400-672 nm) absorption by phytoplankton	$\mu\text{mol}$ photons $\text{m}^{-2} \text{s}^{-1}$
POC	Particulate Organic Carbon	Mass spectrometer	$\mu\text{g L}^{-1}$
PON	Particulate Organic Nitrogen	Mass spectrometer	$\mu\text{g L}^{-1}$
R	Reflectance	Water-leaving radiance / Surface irradiance	$\text{sr}^{-1}$
SRP	Soluble Reactive Phosphate	Continuous flow chemistry	$\mu\text{mol L}^{-1}$
$\varphi_{\text{ph}}$	Quantum efficiency of fluorescence	$(F / \text{PFR}) \times 100\%$	%
$\mu$	Cell specific growth rate between day $_t$ and day $_{t+1}$	$\ln (N_{t+1} / N_t) / (day_{t+1} - day_t)$	$\text{day}^{-1}$
$\mu_{\text{POC}}$	Carbon specific growth rate between day $_t$ and day $_{t+1}$	$\ln (POC_{t+1} / POC_t) / (day_{t+1} - day_t)$	$\text{day}^{-1}$

1 Table 2. *Phaeocystis* chlorophyll-specific absorption coefficients peaks in  $\text{m}^2$  ( $\text{mg Chl}$ ) $^{-1}$   
 2 during exponential and stationary growth. Listed are averages  $\pm$  95% confidence intervals.

Mesocosm number	N	Day	Growth phase	$a^*_{\text{Chl-a}}$ (438 nm)	$a^*_{\text{Chl-c}}$ (466 nm)	$a^*_{\text{Chl-a}}$ (674 nm)
1+2	6	2-4	Exponential	0.053 $\pm$ 0.005	0.044 $\pm$ 0.005	0.026 $\pm$ 0.003
1	4	10-13	Stationary	0.081 $\pm$ 0.012	0.059 $\pm$ 0.003	0.033 $\pm$ 0.004
2	4	10-13	Stationary	0.091 $\pm$ 0.015	0.058 $\pm$ 0.004	0.036 $\pm$ 0.005

3

1 Table 3. Linear regression equations of *Phaeocystis* absorption on HPLC-measured  
 2 chlorophyll-a and -c concentrations. Absorption was calculated with the ARP-4λ-Chla and  
 3 ARP-4λ-Chlc algorithms (eq. 1). Regressions were made for the mesocosms separately, for  
 4 exponential (day 0-4) and stationary (day 5-14) growth phases. Indicated are slope and  
 5 intercepts ± 95% confidence interval.

6

		N	Slope (x 10 <sup>-3</sup> )	Intercept (x 10 <sup>-3</sup> )	R <sup>2</sup>
Chl-a	Mesocosm 1	15	1.2 ± 0.1	-0.6 ± 2.8	0.94
Chl-a	Mesocosm 2	15	1.4 ± 0.2	-3.1 ± 3.5	0.91
Chl-a	Exponential	10	1.4 ± 0.1	-1.3 ± 1.8	0.98
Chl-a	Stationary	20	1.4 ± 0.3	-4.4 ± 5.0	0.82
Chl-a	Stationary*	19	1.4 ± 0.3	-4.6 ± 5.4	0.80
Chl-a	Combined	30	1.3 ± 0.1	-1.8 ± 2.0	0.92
Chl-c	Mesocosm 1	15	1.5 ± 0.2	2.0 ± 6.2	0.88
Chl-c	Mesocosm 2	15	1.7 ± 0.4	-1.0 ± 8.6	0.80
Chl-c	Exponential	10	1.8 ± 0.2	1.3 ± 2.9	0.98
Chl-c	Stationary	20	1.8 ± 0.6	-6.7 ± 14.7	0.59
Chl-c	Stationary*	19	1.6 ± 0.6	-4.0 ± 14.6	0.56
Chl-c	Combined	30	1.6 ± 0.2	0.6 ± 4.9	0.84

7 \*day 9 of mesocosm 1 excluded (1 day after nutrient-spike)

8

1 Table 4. Linear regression equations of *Phaeocystis* fluorescence on HPLC- measured  
2 chlorophyll-a concentrations. Fluorescence was calculated with the FLH-H algorithm (eq. 2).  
3 Regressions were made for the mesocosms separately, for exponential (day 0-4) and  
4 stationary (day 5-14) growth phases. Indicated are slopes and intercepts  $\pm$  95% confidence  
5 intervals.

6

		N	Slope ( $\times 10^{-2}$ )	$R^2$
Chl-a	Mesocosm 1	15	$2.6 \pm 0.4$	0.93
Chl-a	Mesocosm 2	15	$3.4 \pm 0.8$	0.88
Chl-a	Exponential	10	$3.1 \pm 0.8$	0.88
Chl-a	Stationary	20	$1.4 \pm 1.1$	0.27
Chl-a	Combined	30	$2.9 \pm 0.5$	0.81

7

8

1 Table 5. Biochemical characteristics of *Phaeocystis* in the mesocosm compared to published  
 2 data from cultures, unless otherwise indicated. Chl is the sum of chlorophyll-a and -c; Fuco =  
 3 fucoxanthin.

Variable	Unit	Mesocosm	Published/Field	reference
Carbon content	pg cell <sup>-1</sup>	10-40	11	(Rousseau et al., 1990)
Chlorophyll-a	pg cell <sup>-1</sup>	0.1-0.2	0.1-0.3 <sup>a</sup> 1.8 <sup>a</sup>	(Buma et al., 1991)
Chlorophyll-c	pg cell <sup>-1</sup>	0.1-0.2	0.3 <sup>a</sup> 0.8 <sup>a</sup>	(Buma et al., 1991) (Astoreca et al., 2009)
C: Chl-a	g:g	60-500	16-400 <sup>b</sup> 65-111 <sup>c</sup>	(Falkowski et al., 1985) (Sathyendranath et al., 2009)
C: Chl	g:g	30-200	-	-
Chl-c: Chl-a	g:g	1.1-1.9	0.1-0.8 <sup>e</sup> 0.4 0.4	(Buma et al., 1991) (Astoreca et al., 2009) (Seoane et al., 2009)
Fuco: Chl-a	g:g	1.2-2.2	0.2-0.3 <sup>d</sup> 0.3-0.8 <sup>e</sup> 0.3-1.0 <sup>d</sup>	(Astoreca et al., 2009) (Buma et al., 1991) (Seoane et al., 2009)

4 <sup>a</sup>for larger non-flagellated *Phaeocystis* cells

5 <sup>b</sup>range of 3 species cultured at different irradiances

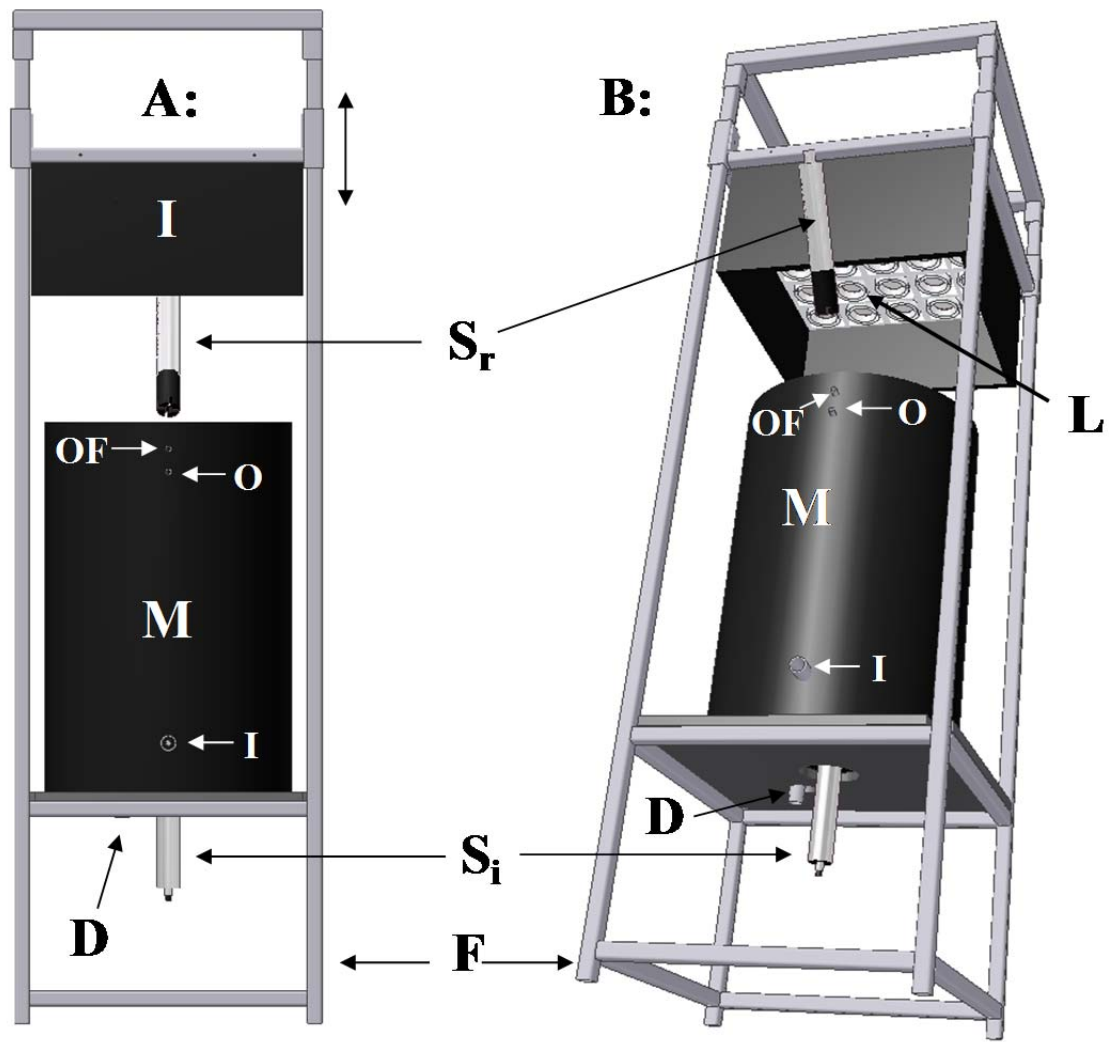
6 <sup>c</sup>C : Chl-a for prymnesiophytes in field samples determined by regression analysis

7 <sup>d</sup>high value at low irradiance

8 <sup>e</sup>in Marsdiep during *Phaeocystis* blooms (Wadden Sea tidal inlet)

9

10



1 **1 meter**

2 Figure 1. Schematic representation of the mesocosm system. A. side view, B. view from

3 below. The mesocosm vessel (M, height 0.75 m, diameter 0.50 m) is placed inside a metal

4 frame (F) that also holds the illumination-box (I). The illumination-box contains 25 Solux™

5 lamps (L) and is height-adjustable. Two hyperspectral sensors were installed: one for bottom

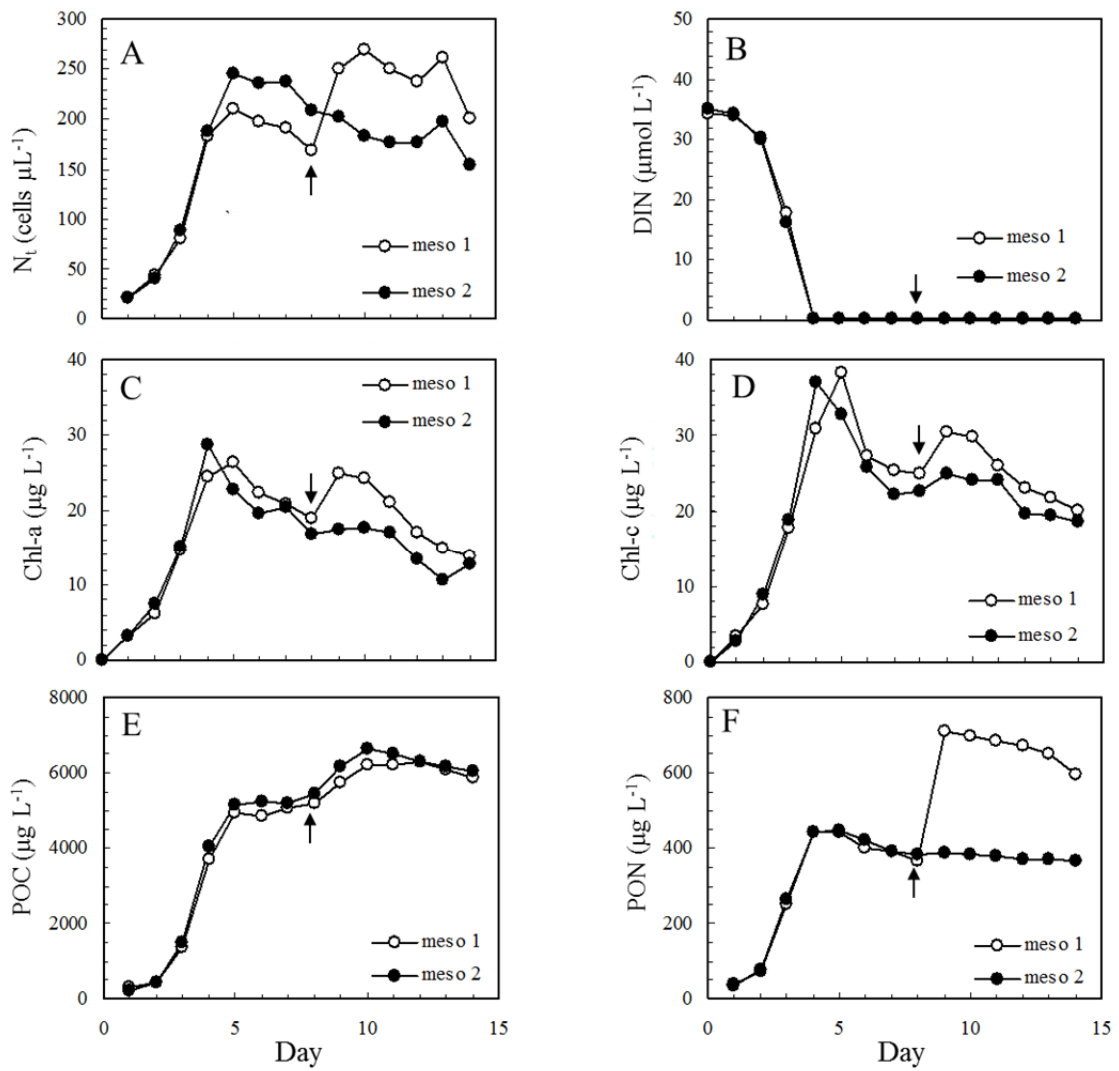
6 irradiance (Si) and one for water-leaving radiance (Sr). Water was pumped round through an

7 outlet at -0.10 m (O) and an inlet (I) at +0.10 m from the bottom. An overflow (OF) at -0.05

8 m was used to keep the water level constant. The mesocosm is emptied with a drain (D) in the

9 bottom. For clarity, the construction holding the radiance sensor (Sr), electrical wiring, tubing,

10 valves and pump are not shown.



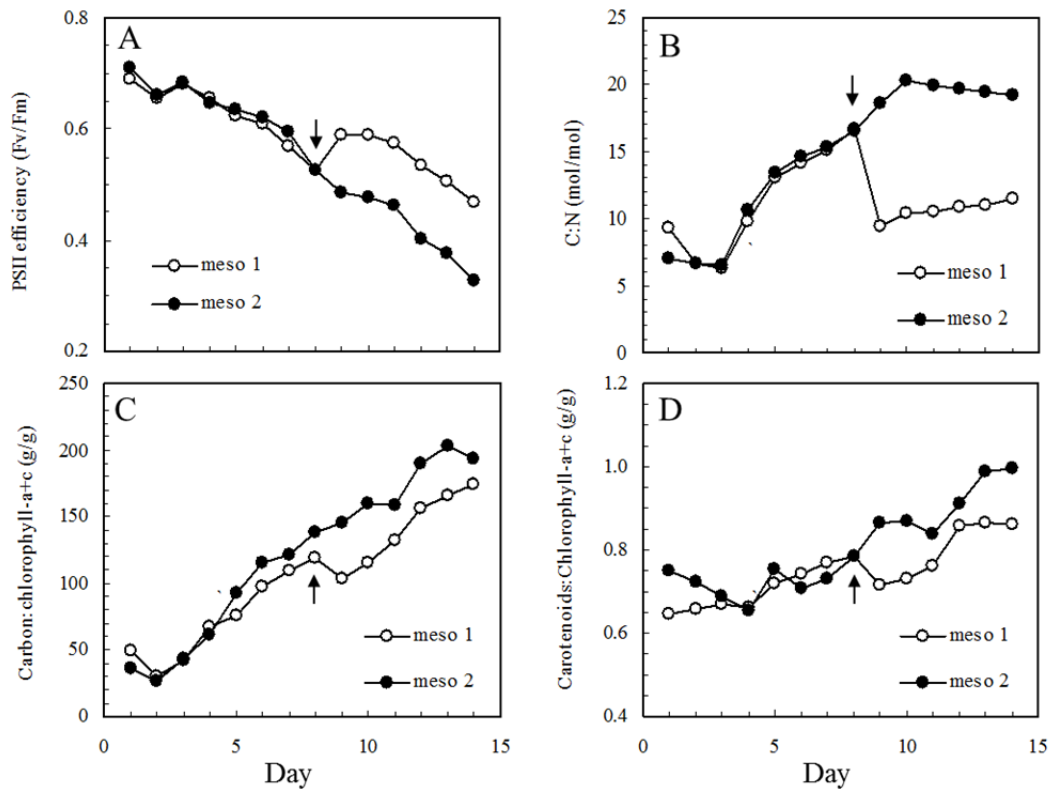
1

2 Figure 2. A-F. *Phaeocystis*, nutrient and carbon dynamics in two mesocosms (meso  
 3 meso 2) in time. A. Cell abundances (cells  $\mu\text{L}^{-1}$ ), B. Dissolved Inorganic Nitrogen (DIN,  $\mu\text{mol L}^{-1}$ ),  
 4 C. Chlorophyll-a (Chl-a,  $\mu\text{g L}^{-1}$ ), D. Chlorophyll-c (Chl-c,  $\mu\text{g L}^{-1}$ ), E. Particulate Organic  
 5 Carbon (POC,  $\mu\text{g L}^{-1}$ ), F. Particulate Organic Nitrogen (PON,  $\mu\text{g L}^{-1}$ ). The arrow indicates the  
 6 nutrient addition to mesocosm 1 after sampling on day 8.

7

8

9



1

2 Figure 3 A-D. *Phaeocystis* physiology and pigment ratios in two mesocosms in time. A.  
3 Photosystem II efficiency (Fv/Fm), B. Carbon to Nitrogen ratio (C : N, mol mol<sup>-1</sup>), C. Carbon  
4 to Chlorophyll a + c ratio (C : Chl-a+c, g.g<sup>-1</sup>), D. Carotenoids to Chlorophyll a + c ratio (g.g<sup>-1</sup>). The arrow indicates the nutrient addition to mesocosm 1 after sampling on day 8.

6

7

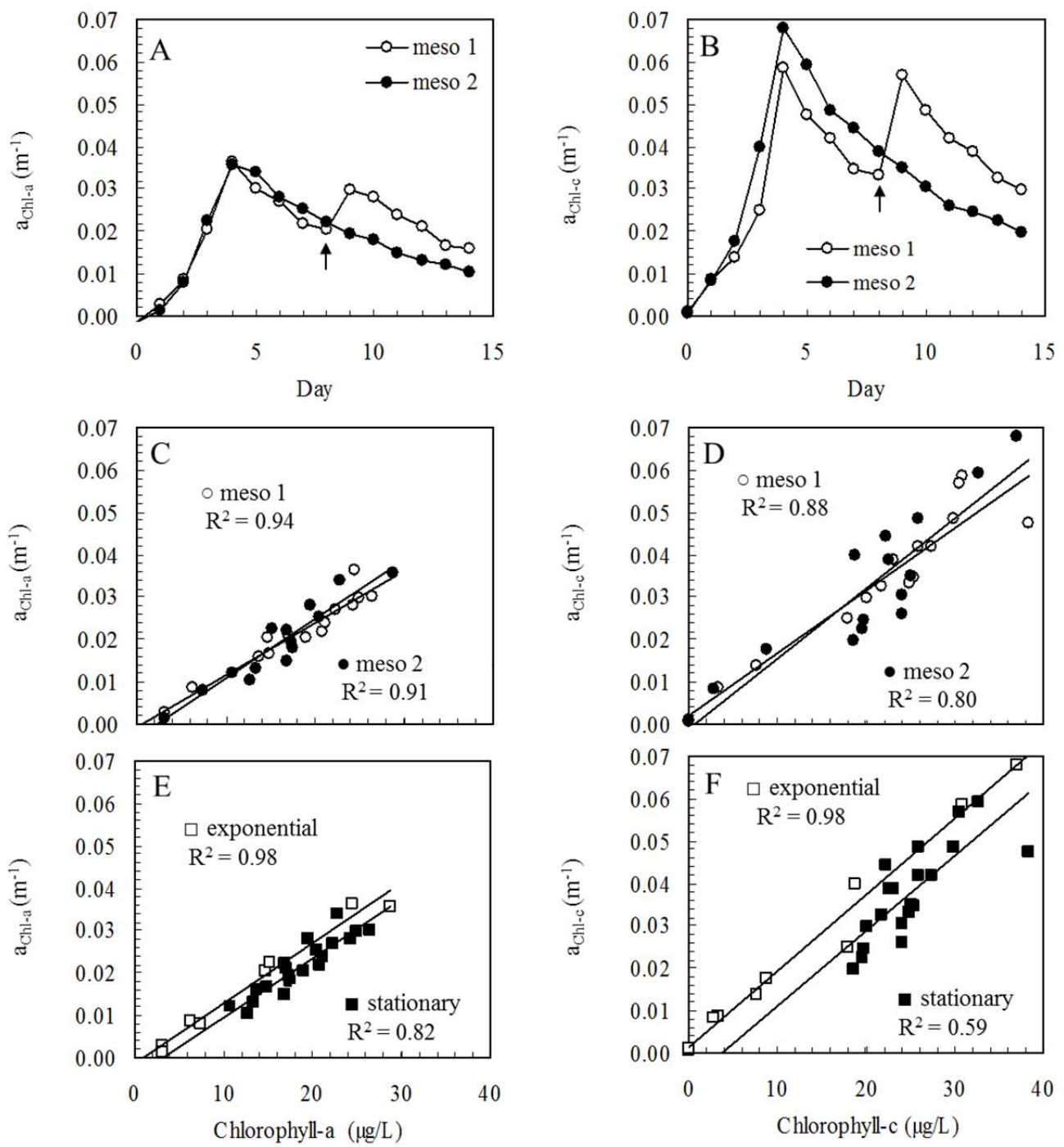
8

9

10

11

12



1

2 Figure 4 A-F. Absorption characteristics in *Phaeocystis*. A-B: Temporal development (days)  
 3 of absorption by chlorophyll-a ( $a_{Chl-a}$ ,  $m^{-1}$ ) and -c ( $a_{Chl-c}$ ,  $m^{-1}$ ) calculated from reflectance  
 4 spectra in both mesocosms. C-F: linear regression of absorption on chlorophyll-a and -c ( $m^{-1}$ )  
 5 against Chl-a and Chl-c concentrations ( $\mu g L^{-1}$ ) was performed separately for both mesocosms  
 6 (C, D) and for exponential and stationary growth phases (E, F).

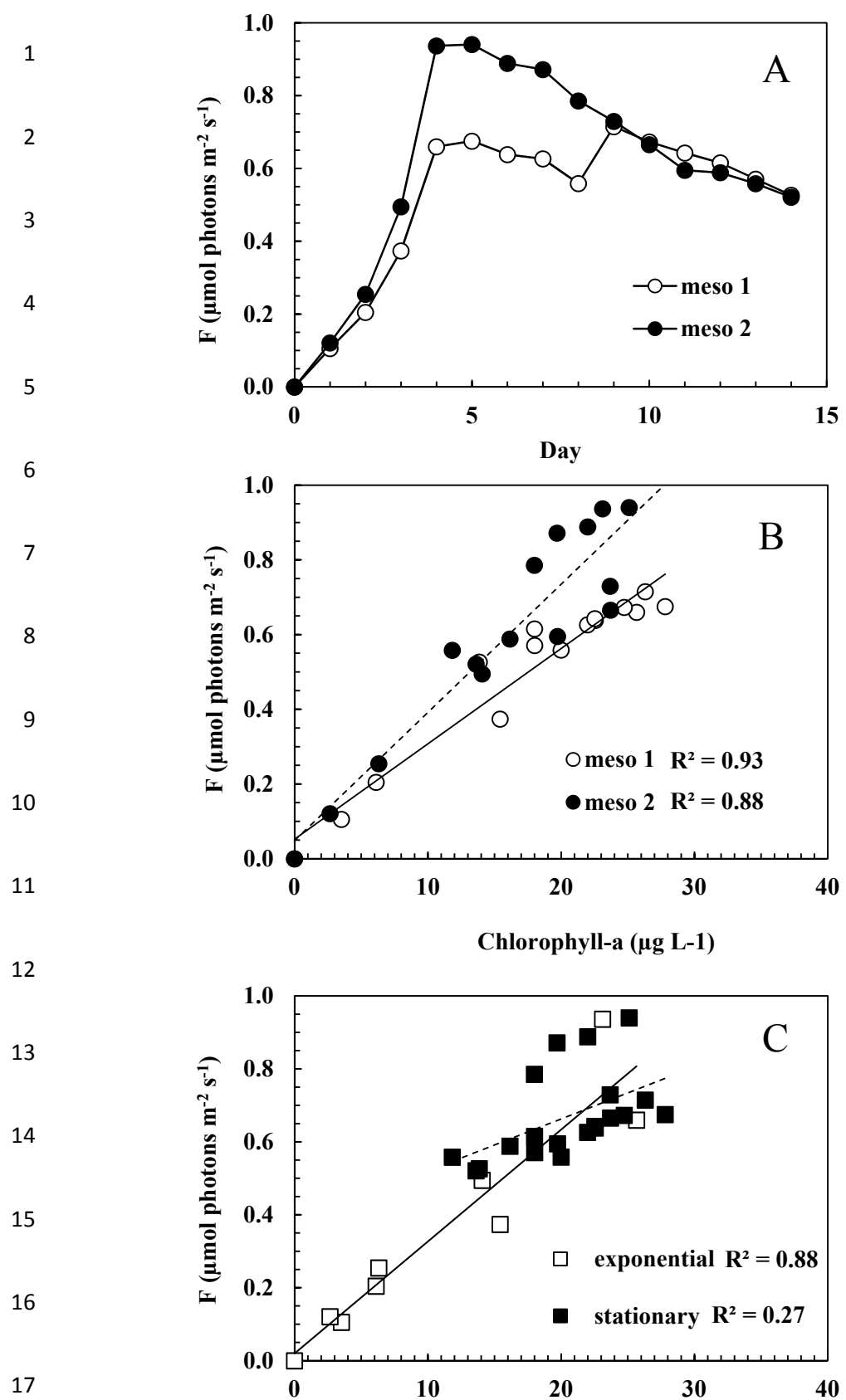
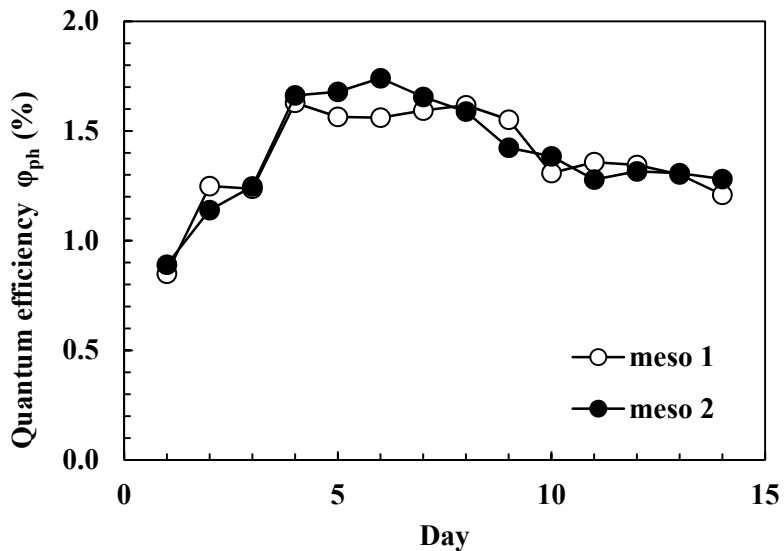


Figure 5 A-C. Fluorescence emission. A: Daily development of the fluorescence emission near 682 nm ( $F, \mu\text{mol photons m}^{-2} \text{s}^{-1}$ ) calculated from reflectance spectra, B: linear

- 1 regression of fluorescence ( $F$ ,  $\mu\text{mol photons m}^{-2} \text{ s}^{-1}$ ) on chlorophyll-a ( $\mu\text{g L}^{-1}$ ) for both
- 2 mesocosms separately and C: for both exponential and stationary growth phases.

3



1

2

3     Figure 6. Development in time (days) of quantum efficiency  $\varphi_{ph}$  derived from total  
4     phytoplankton absorption and fluorescence in two mesocosms.

5

6

7

8

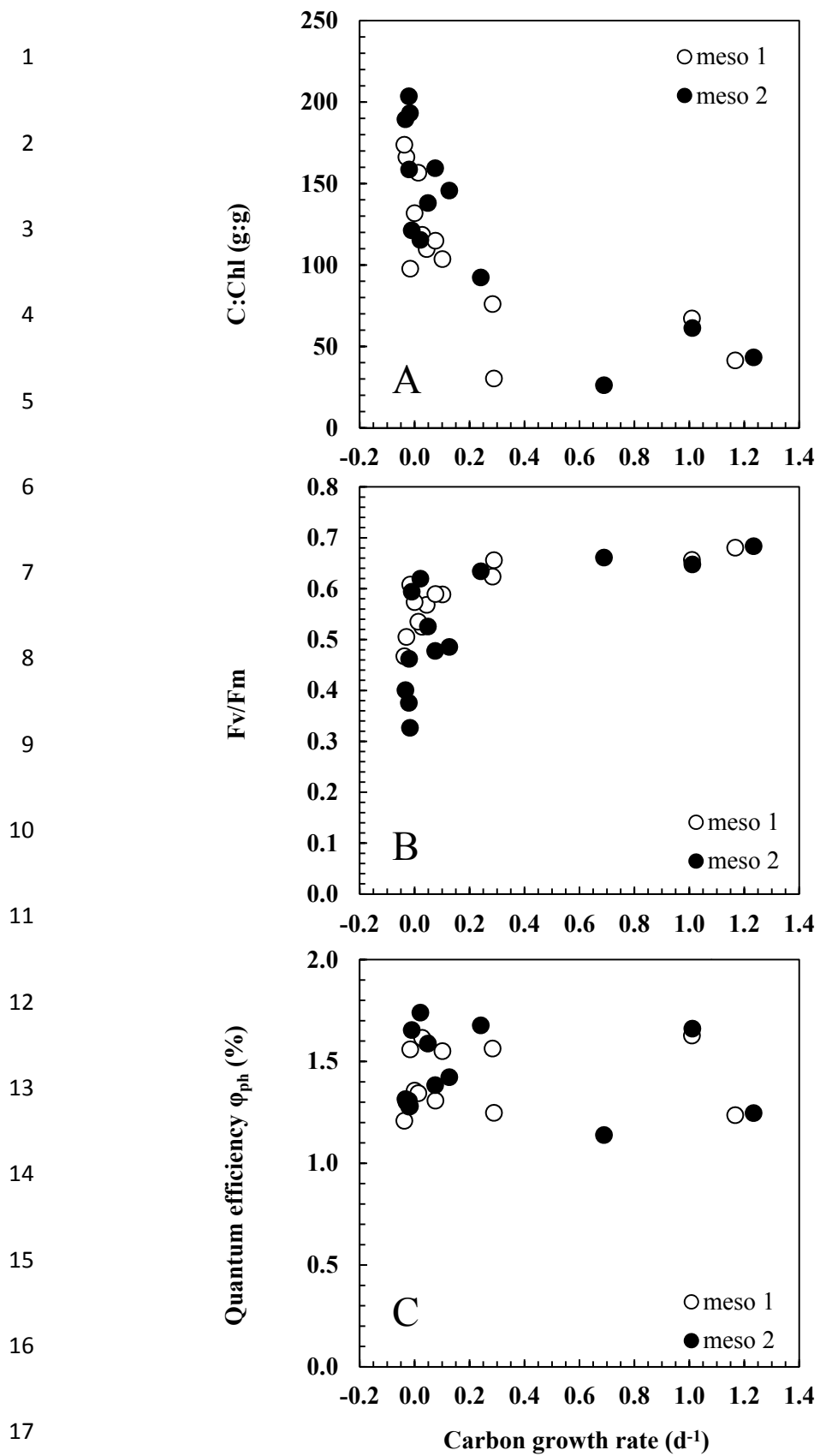
9

10

11

12

13



1 Figure 7. Three proxies for growth rate as function of measured carbon growth rate ( $\mu_{POC}$ ,  $d^{-1}$ )  
2 A: Carbon to Chlorophyll a+c ratio (C : Chla+c,  $g\ g^{-1}$ ), B: Photosystem II efficiency  
3 (Fv/Fm) and C: Quantum efficiency ( $\phi_{ph}$ , %). Data combined from both mesocosms.

4